SUBMISSION TO
GEODERMA

DATE 23RD MARCH 2021
Written: August 2020

TITLE:
On the utilization of mica waste: the pore-fluid chemistry of mica soils and its implication for erosion susceptibility

AUTHORS:
CORRESPONDING AUTHOR:
Mr Christopher U. Ibeh
Department of Civil and Environmental Engineering
University of Strathclyde
James Weir Building - Level 5
75 Montrose Street - Glasgow G1 1XJ, Scotland, UK
E-mail : christopher.ibeh@strath.ac.uk

Dr. Matteo Pedrotti
Department of Civil and Environmental Engineering
University of Strathclyde
James Weir Building - Level 5
75 Montrose Street - Glasgow G1 1XJ, Scotland, UK
E-mail : matteo.pedrotti@strath.ac.uk

Prof. Alessandro Tarantino
Department of Civil and Environmental Engineering
University of Strathclyde
James Weir Building - Level 5
75 Montrose Street - Glasgow G1 1XJ, Scotland, UK
E-mail : alessandro.tarantino@strath.ac.uk

Prof. Rebecca J. Lunn
Department of Civil and Environmental Engineering
University of Strathclyde
James Weir Building - Level 5
75 Montrose Street - Glasgow G1 1XJ, Scotland, UK
E-mail : rebecca.lunn@strath.ac.uk

KEYWORDS
Mica Soil, erosion, sedimentation, pore-fluid-chemistry, Jet erosion test, circular economy

Number of words: 8338
Number of figures: 13
Number of tables: 2

On the utilization of mica waste: the pore-fluid chemistry of mica soils and its implication for erosion susceptibility

Abstract

Soil is a vital resource which is limited in availability and must be adequately managed for sustainable development. Despite the importance of soil and its limited availability, a huge amount of soil is classified as waste. As one of the world's largest soil waste generators, the mining industry must transition to a circular economy model to meet sustainability requirements. As a readily available, large-volume waste material (about 10 million tonnes each year), waste mica has been considered for re-use as an alternative soil potassium source for plants, as landscaping material etc. One of the problems with mica waste is its susceptibility to erosion. To use mica as an agricultural or landscaping material, it is therefore important to understand the erodibility of mica and how its erodibility can be reduced. This study presents an experimental campaign to characterize mica erosion susceptibility. Mica particle-to-particle interaction forces and their effect on the macroscopic material behaviour were systematically investigated by changing pore fluid pH and ionic concentration. Sedimentation and liquid limit tests were first carried out to inform a conceptual model of the mica fabric. Triplets of 12 mica samples, compacted at different water contents and with different pore chemistry, were tested for erosion susceptibility using a Jet Erosion Test (JET) apparatus. The particle configuration of mica samples consistently varied with the pore water chemistry, regardless of whether the samples being tested were suspension sediments or compacted samples. For mica samples formed with neutral water at low ionic concentration, the particles are in a dispersed configuration. This implies a poor mechanical behaviour and high erosion susceptibility, as particles are eroded one by one. For porewater samples formed with an increased ionic strength

or within the acidic pH range, particles tend to cluster together and organize in a non-dispersed configuration. This results in an improved mechanical behaviour and less erosion susceptibility, as group of particles must be eroded as opposed to individual ones. Similarly, the Jet erosion test results reinforced these observations showing that mica erodibility varies with porewater chemistry. Considering that mica erodibility varies with pore fluid chemistry and mica waste derived from mining operations are often slightly acidic, this paper paves the way for tailored assessments of individual mica waste materials to determine the appropriateness of their use.

Key words: Muscovite-Mica, erosion, sedimentation, pore-fluid-chemistry, Jet erosion test, circular economy

1 Introduction

Soil is a vital resource which connects essential spheres such as food security, biodiversity, climate change and public health, as well as other social, economic, and environmental aspects of life. It is however limited in quality and availability and needs to be responsibly managed to meet the sustainable development goal (Keesstra et al., 2016; H. Wang & Zhang, 2021). Despite the importance of soil and its limited availability, huge amounts of soil are classified as waste. It is estimated that approximately 15 Gt/yr of waste soil is generated by the mining industry globally (Lottermoser 2010). As one of the world's largest waste generators, the mining industry must transition to a circular economy model to improve its sustainability.

Within the mining industry, the management of mica waste has generated significant attention due to the large volume generated. Mica waste originates from mining of relatively valuable materials such as gold, copper, uranium and platinum (Nosrati et al., 2009), from mining of

coarse material such as granite (Hojamberdiev et al., 2011) from the mining of other phyllosilicates such as China clay (Zografou et al., 2014) and from the mining of mica itself (Basak, 2019). For instance, China clay extraction and processing involves the production of a very large quantity of mica waste, typically for every tonne of china clay, one tonne of residual mica is produced. About 10 million tonnes of mica waste is generated in a year and over 600 million tonnes of total industry stockpile is estimated to be available (Palumbo-Roe et al., 2014). Mica waste is usually deposited in large lagoons and abandoned in clay pits. It contains between 10% and 75% mica and currently has seen very limited re-use; within flux for ceramic glazes and as a mild abrasive (Basak, 2019; Hojamberdiev et al., 2011; Zografou et al., 2014). As a readily available, large-volume material, waste mica has been considered for use as backfill material and a landscaping material (Dudeney et al., 2013; Karlsson et al., 2017). Mica has also been considered for re-use as a component of construction materials, such as bricks or cement (Cresswell and Sims 2007) and in the agricultural industry as a source of important soil nutrients such as potassium which plays an important role in several physiological processes in plant nutrition (Meena et al., 2015; Singh et al., 2010).

A major problem with mica waste is that the material is susceptible to erosion as highlighted by **Sinha et al. (2017)**. One of the key questions to be addressed in order to access the suitability of mica as an agricultural or backfill material is how erodible the mica is and how its susceptibility to erosion can be reduced. This issue is addressed by this paper.

Mica is a brittle rock, comprised of clay minerals, with a layered or platy texture. The charge on mica particles is well documented to be pH dependent (van Olphin 1977, Nishimura *et al.*, 1992; Mitchell and Soga, 2005; Gratchev and Towhata, 2013; Liu *et al.*, 2018) and affects their erodibility (Man and Graham, 2010; Momeni et al., 2020). Similarly, the use of mica waste for example, as an alternative source of potassium may require the addition of organic matter to promote the K mobilization to soil solution and its absorption by the plant (Bakken et al., 1997;

Basak, 2019; Basak et al., 2017; A. Wang et al., 2015). This process gives rise to the production of organic acids (Biswas & Basak, 2014), which reduces the pH of the medium. Hence, to characterise the erodibility of mica waste it is important to consider a wide range of soil porewater chemistries.

This paper presents an experimental campaign to characterize mica erosion susceptibility for a range of porewater chemistries. Triplets of 12 mica samples, compacted at different water contents and with different pore chemistries, are tested for erosion susceptibility using a Jet Erosion Test (JET) apparatus and erodibility is found to vary with porewater pH. Results from sedimentation tests and liquid limit tests are used to inform development a conceptual model of particle-to-particle interactions. This model is able to explain the observed variations in the erosion resistance of mica under varying pore-water chemical conditions.

1.1 Mica

Mica may occur as muscovite, lepidolite, phlogopite, biotite, and lepidomelane mineral form (Hoseini et al., 2016). Muscovite mica is used in this study due to its ubiquitous nature. Mica is a phyllosilicate mineral, which may range in size from sand to silt and clay size platy particles, but it occurs mostly as a silt sized waste material in mine settings. It has the fundamental formula $KAl_2(AlSi_3O_{10})(OH)_2$ and is a 2:1 clay mineral (Figure 1). The crystal structure is the one of active clays, it comprises a stack of unit layers of an Al–O–Al octahedral (O) layer sandwiched between two Si–O–Al tetrahedral (T) layers. Substitutions of lattice Si^{4+} by Al^{3+} in the tetrahedral layer and Fe^{3+} or Mg^{2+} and Ca^{2+} for Al^{3+} in the octahedral layer which invariably occur, result in a permanent net negative charge on the basal clay mineral (Figure 1). The charge deficiency is compensated by interlayer cations such as K^+ and Na^+ adsorbed between the T-O-T sheets, fitting closely into the hexagonal holes of the Si–O–Al sheet. The interlayer cations (e.g. K^+) strengthen the bonding between basal planes of TOT sheets, which

are normally held by attractive van der Waals forces, through the attractive electrostatic interactions (Nosrati et al., 2009).

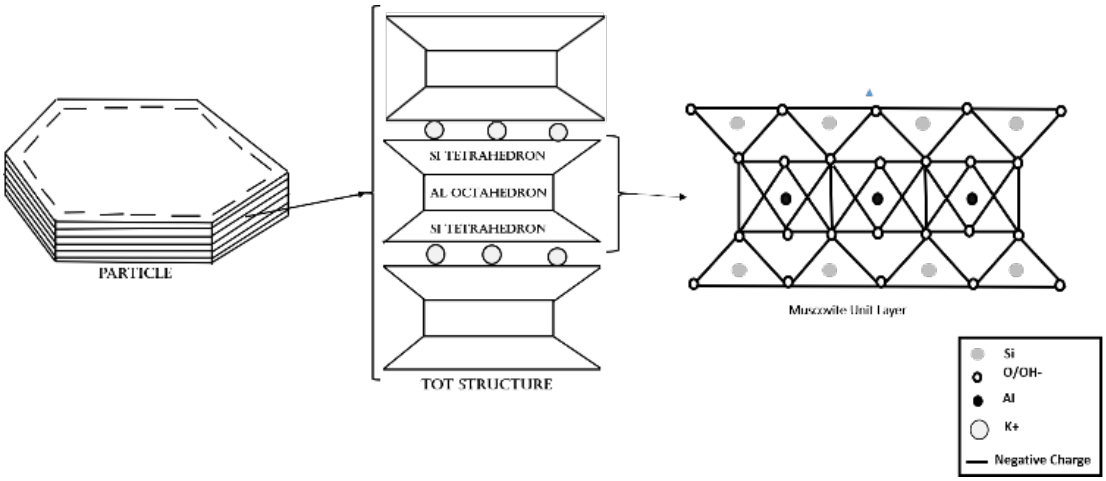

Figure 1: Muscovite mica structure

2 Materials and Methods

Muscovite mica silt purchased from LKAB minerals LTD, UK was used for this study. Laser diffraction analysis (Figure 2) showed the muscovite silt to have an equivalent average grain size of about 30 µm. The muscovite specific gravity is 2.8 (given by LKAB).

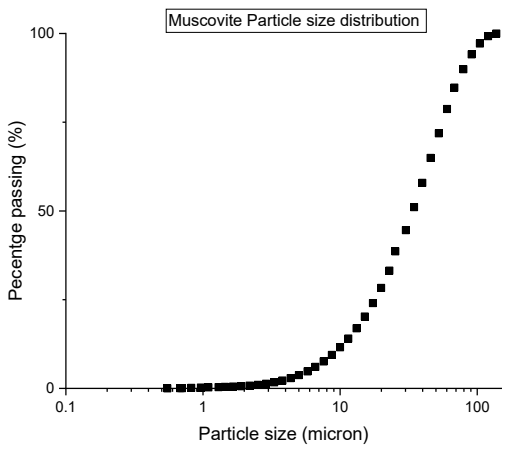

Figure 2: Particle size distribution of muscovite mica

To characterize the muscovite chemical composition, Micro-X-ray fluorescence (XRF) was performed at Bruker AXS, Germany using M4 Turnado Micro-XRF Spectrometer. The XRF analysis (Table 1) showed that the muscovite silt contains predominantly Al_2O_3 (32% wt.), SiO_2 (43% wt.), K_2O (13% wt.) Fe_2O_3 (8% wt.) and trace amounts of Na_2O and other compounds.

Table 1. Chemical composition of the muscovite silt used in this study

Element	**Atomic Number**	**Compound**	**Normalised Stoichiometric Composition (wt.%)**
Mg	12	MgO	0.557
Al	13	Al_2O_3	32.706
Si	14	SiO_2	43.612
K	19	K_2O	13.01
Ti	22	TiO_2	1.103
Mn	25	MnO	0.018
Fe	26	Fe_2O_3	8.399
Co	27		0.022
Ni	28	NiO	0.002
Zn	30	ZnO	0.007
Ga	31		0.011
Rb	37		0.06
Sr	38	SrO	0.003
Y	39	Y_2O_3	0
Zr	40		0.051
Nb	41		0.015
Ba	56	BaO	0.082
Rh	45		0

2.1 Specimen Preparation

Each sample of mica underwent a standard preparation procedure comprised of a washing stage and a pH correction stage.

Washing stage: As shown by the XRF analysis (Table 1), the muscovite is dominantly composed of potassium ion. The muscovite was rendered mono-ionic by using KCl. A procedure similar to the one outlined by van Olphen (1977), and Palomino and Santamarina, (2005) was adopted. The muscovite was mixed with a 2 mol/L KCl solution at -3 mL of solution per gram of Muscovite. The suspension was left for 48 h, during which the clay particles were allowed to settle. Subsequently, its supernatant was siphoned and replaced with 1mol/L KCl. After 24 hours the supernatant was siphoned again and replaced with a fresh 1mol/L KCl and left to equalize for 96 hours. Thereafter, the excess salt was removed through 10 washing cycles with deionized water. The muscovite was then oven dried and ground into powder using a mortar and pestle and was eventually passed through a 425-micron sieve.

pH correction stage: when the muscovite is mixed with distilled water, the mixture result in a pH of ~8. Muscovite has the capacity to buffer the pH of acidic solutions. To have mica slurries or suspensions at a different pH, the pH needs to be corrected in the muscovite-water mixture, to neutralize the buffering effect of the mica. Depending on the target pH, the muscovite batches were corrected by adding drops of diluted HCl acid or KOH base to respectively increase or decrease the pH of the mixture. In the case of bases, a KOH solution was preferred to a NaOH solution to preserve the nature of the cations (K^+) dispersed in the mica mixture. In both cases (acidic or alkaline batch), the mixture was left to equilibrate for at least 24 hours and in case, the pH was corrected again.

For the sedimentation tests, samples at 4 different pH (e.g., 3, 5, 7, 9) were respectively prepared at 4 different KCl concentrations: 0 mol/L, 0.003 mol/L, 0.1 mol/L and 1.8 mol/L. A 2.54 cm diameter acrylic cylinder filled with the pore fluid and the Muscovite at a water content of ~1800 and total suspension volume of 78ml was used. The suspension was mixed and left to equilibrate overnight, after which it was remixed.

For liquid limit tests, samples at two different pH (5 and 8) were tested. The pH 8 sample was prepared using demineralized water and hence did not require any pH adjustment since the muscovite mixed with demineralized water gave a pH of about 8. The sample at pH 5 was instead prepared as described above.

For the JET erosion test, two sets of samples, at pH 5 and pH 8, were prepared with different initial water contents (e.g., 0.2, 0.3 and 04) and statically compacted at 90 kPa in a cylindrical mould of 10cm in diameter by 10 cm in height. As compacted samples are partially saturated, adjusting the pH at low water content would result in improper mixing and heterogeneous areas within the sample. A different procedure than the one described above was implemented to reach the target pH for each sample. A slurry of mica (w=1.5) was initially prepared at either pH 5 or 8 following the same methodology described in the above paragraph pH correction stage. The pH-corrected slurry was then oven dried (24 hours at 105 °C) and then ground with a pestle and mortar. In this way, the dry clay was already in equilibrium, when exposed to water of the same pH, and the buffering effect of mica was neutralized. Therefore, the dry mica was mixed with a given amount of water at the target pH and then statically compacted. After compaction, each sample was subsequently kept in a sealed nylon bag for 48 hours to homogenize. Each sample was prepared in triplicate, resulting in a total of 18 samples.

2.2 Experimental procedure

2.2.1 Sedimentation test

For the sedimentation tests, the following procedure was followed. First, the soil suspension with the target pH and electrolyte concentration was gently poured into the acrylic cylinder, and then it was covered, repeatedly inverted for 2 minutes, placed on a level surface and the time recorder simultaneously started. During the sedimentation test, the clear water-clay suspension interface was recorded (ruler accuracy of 1mm), when visible, otherwise the

sediment height was recorded instead. The height was recorded, starting from 2 seconds, and subsequently samples doubled the time, until there was no significantly measurable difference between three subsequent measurements. At the end of the test, the supernatant fluid was siphoned off, and the pH measured. As both the final volume of the sediment and the dry mass of the sample were recorded, the final void ratio of each sediment could be calculated.

2.2.2 Liquid Limit test

The liquid limit test was conducted with a penetrometer in accordance with BS Code (1990). However, as described in the previous section, the samples were prepared with different pore fluid chemistries (pH 8 and pH 5, no electrolyte added). Penetration measurements were obtained for five moisture contents and the moisture content corresponding to 20mm penetration was recorded as the liquid limit.

2.2.3 Jet Erosion Test

A schematic of the JET erosion apparatus used is shown in Figure 3. The custom-made JET erosion apparatus (Beber et al., 2019) was recently created in the Geomechanics laboratories at the University of Strathclyde and was designed according to **Hanson & Cook, (2004)** to investigate the erodibility and strength of compacted muscovite at varying porewater pH (pH 5 and pH 8) and moisture content (0.20, 0.30 and 0.40). The jet erosion test was performed using the following parameters: an initial nozzle height from the sample surface, J_E, of 80 mm and a nozzle diameter (d_0) of 6.4mm.

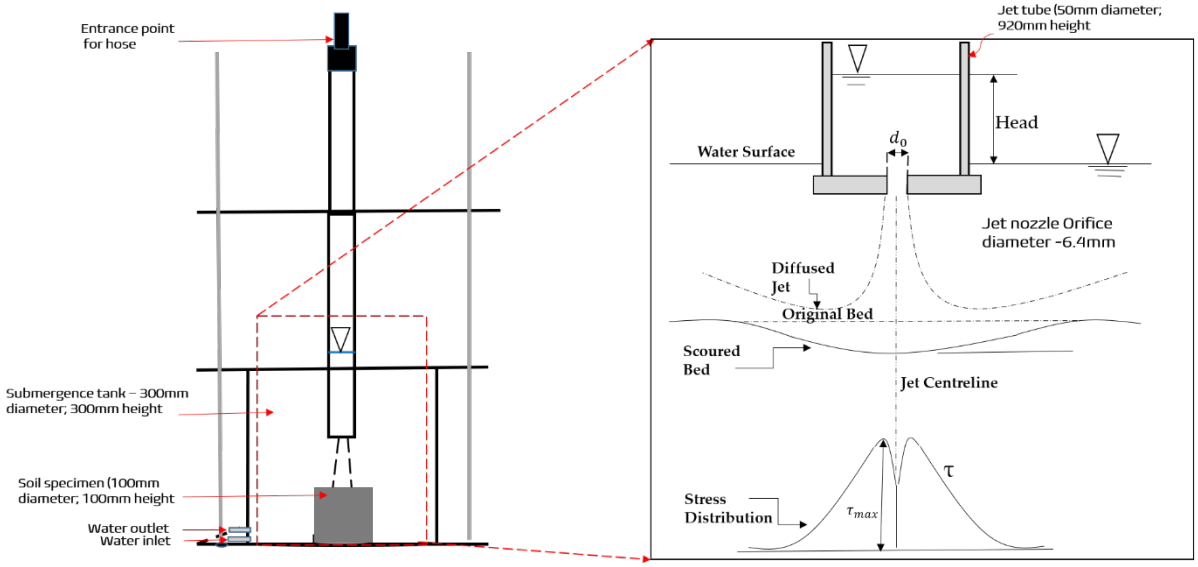

Figure 3: Schematic of jet erosion apparatus at the University of Strathclyde (modified from Hanson & Simon, (2001)*).*

In Figure 4 the workflow of the erosion test experimental procedure is reported.

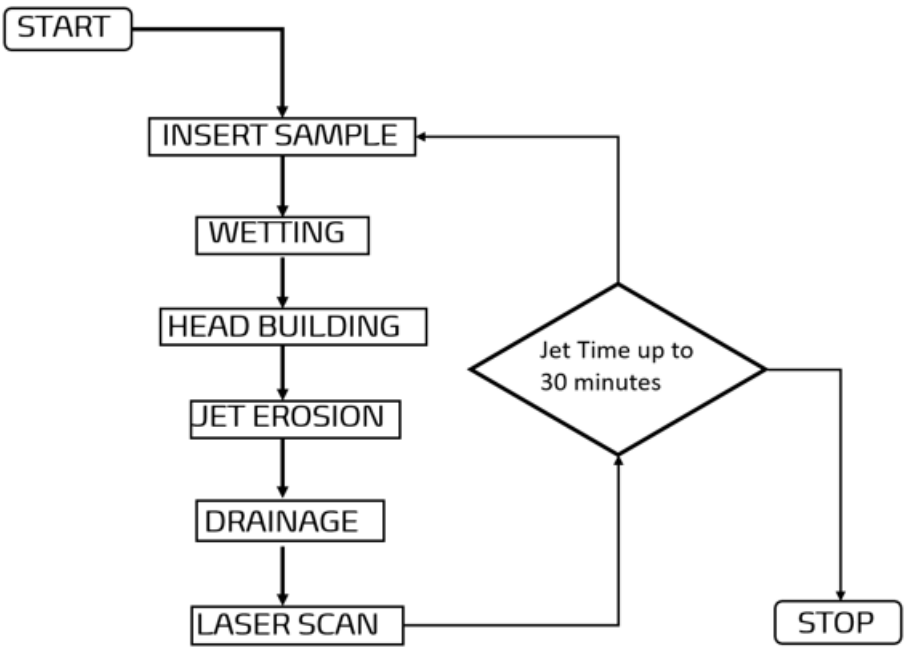

Figure 4: workflow showing the procedure for the conduct of the JET erosion test

Stage 1: Sample insertion

The prepared cylindrical soil sample (labelled as soil sample mould in Figure 4) is tightly secured at the base of the tank onto a protruding ring.

Stage 2: Wetting

Water is piped into the tank through the water inlet positioned at the bottom (Figure 3) until the sample is submerged (~ 1 minute).

Stage3: Head building

The water head inside the "jet tube" (Figure 3) is increasingly raised, until a constant hydraulic had of 130 mm is reached.

Stage4: Jet Erosion

Once the target water head was reached, the jet tube was opened via a deflector and the jet test started. The jet was kept on for 5 minutes at a constant hydraulic head, after which, the jet tube was closed again.

Stage 5: Drainage

Once the jet tube was closed, the cell was drained (~2 minutes) from the outlet valve positioned at the bottom of the cell (Figure 3), in order to allow removal of the sample.

Stage 6: Laser scan

To allow for accurate determination of the scour depth, a 2D/3D scan control 2700-100/BL from Micro-Epsilon laser scanner was used. The scanner was mounted on a movable frame coupled with a software-timed motion controller OWIS PS-II. The scanner reference resolution is 15 microns. After scanning the sample surface, the whole procedure from stage 1 was then repeated, until a total elapsed erosion time of 30 minutes was reached. For each 5-minute step, the maximum scour depth and the total eroded volume was recorded. The critical stress, τ_C,, was then determined in accordance with **Hanson & Cook, (2004).**

3 Results and Discussion

3.1 Sedimentation test

To investigate the microstructural behaviour of muscovite at low density, muscovite suspensions with different pore chemistries were tested. Among the different samples two clear patterns could be distinguished depending on the pore chemistry.

As illustrated in Figure 5, two types of behaviour were observed: one with a clear water-suspension interface (Figure 5a) and the other with a clear sediment deposition height interface (Figure 5b). In the samples with clear water – suspension interface, once the sedimentation had started, the interface descends with time. Simultaneously, a sediment layer accumulates at the bottom of these samples, but the sediment interface height is not visible enough for measurement. These samples are said to be non-dispersive and only the visible clear water-suspension interface is measured and reported as shown in figure 6 (the interface decreases with time).

By contract, for samples with clear sediment deposition height interface (dispersive samples), their water -suspension interface is not visible enough for measurement. Only the clear sedimentation deposition height interface was measured and reported. This interface increased with time as shown in figure 6. In Figure 5a and b, the sediment deposition height interface is highlighted in blue and the clear water – suspension interface is highlighted in orange. The two interfaces converge into a single interface at the end of the sedimentation.

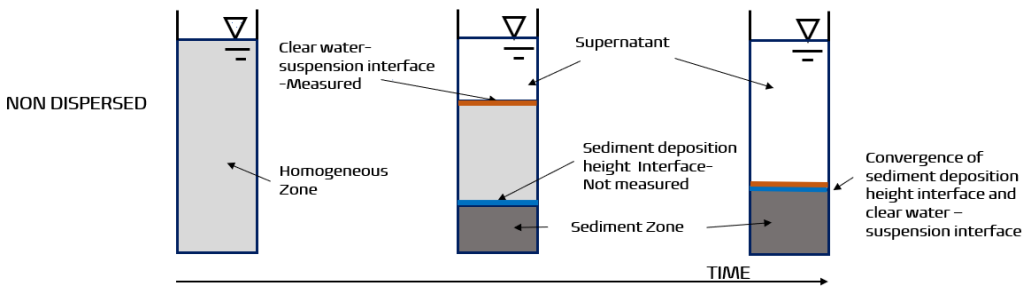

5a)

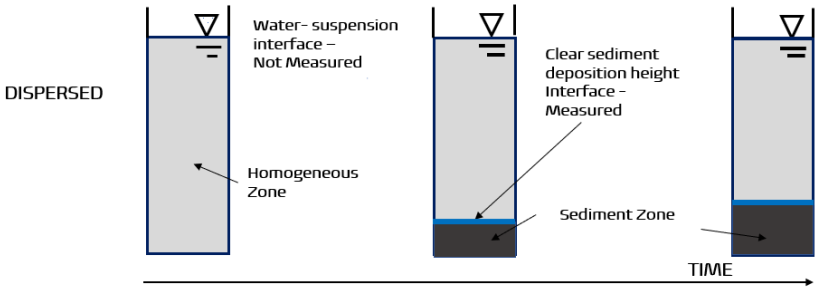

5b)

Figure 5: Illustration of different sedimentation patterns: a) non-dispersed sedimentation pattern showing two distinct interfaces, supernatant-suspension interface, and suspension-sedimentation zone interface; b) dispersed sedimentation pattern showing only the sedimentation zone-suspension interface.

In Figure 6, the data acquired from the sedimentation tests illustrated in Figure 5 (for pH 3, 5, 7 and 9 and KCl concentrations of 0 mol/L, 0.003 mol/L, 0.1 mol/L and 1.8 mol/L) are reported. Figure 6a shows two muscovite suspension sedimentation curves with no electrolyte concentration (0 mol/L KCl) at pH 3 and 9. The pH 3 sample showed a non-dispersed behaviour. The clear water – clay suspension interface was visible (Figure 6a) and decreased with time from 18cm to 3cm. A steep decline in the interface height is observed between 2 minutes and 15 minutes after the start time. Beyond 15 minutes, the interface height was stable at about 3 cm and did not change further (the final sedimentation height after 30 minutes is presented in table 2 below). For the sample at pH 9, a dispersed behaviour was observed; there was no visible clear water - clay suspension interface. The sediment height interface increased from zero at the start, to about 2cm after 11 minutes after which it was relatively stable. At the end of the sedimentation, samples had final void ratios of 4.4 and 2.6, for pHs of 3 and 9 respectively.

Table 2: Final sedimentation height after 30 minutes

	Final sedimentation height (cm)			
	pH 9	pH 7	pH 5	pH 3
1.8Mol/L KCl	2.76	2.99	2.99	3.105
0.1Mol/L KCl	2.99	2.99	2.99	3.105
0.003Mol/L KCl	2.07	2.07	3.105	3.22
0Mol/L KCl	1.84	1.91	3.2	3.22

Figure 6b shows the sedimentation curves of 4 samples with an electrolyte concentration of 0.003 mol/l KCl, but with different pH (3, 5, 7 and 9). The pH 3 and pH 5 samples showed a non-dispersed behaviour (Figure 6b), with a similar trend to that of pH 3 with no electrolyte concentration (Figure 6a), while the pH 7 and pH 9 samples showed a dispersed behaviour (Figure 6b) similar to that of pH 9 with no electrolyte concentration (Figure 6a). Figure 6c shows the sedimentation curve for all four samples with an electrolyte concentration of 0.1 mol/l KCl and varying pH. In this case, regardless of pH, the behaviour is non-dispersed. Finally, Figure 6d shows the sedimentation curves for all samples with an electrolyte concentration of 1.8 mol/l KCl. Again, all samples show a non-dispersed behaviour, regardless the pH.

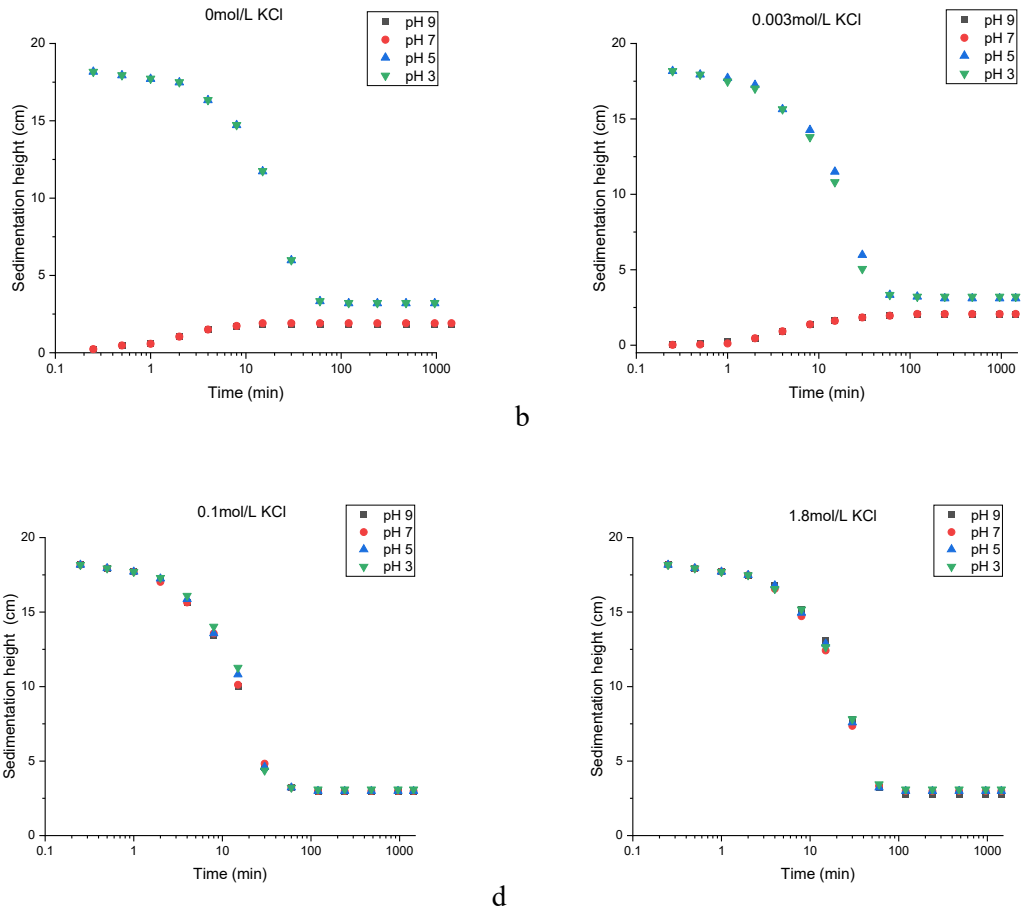

Figure 6: Muscovite sedimentation trend for different pH and ionic concentration at a) 0 mol/l KCl b) 0.003 mol/l KCl c) 0.1 mol/l KCl and d) 1.8 mol/l KCl

3.2 Liquid Limit test

To estimate the mechanical strength of the muscovite under different particle configurations (dispersed or non-dispersed), the liquid limit of the muscovite was determined at two different pH. In Figure 7 the two liquid limit tests are reported. Mica prepared at pH 8 (dispersed particle configuration) had a liquid limit of 60% whereas the mica sample prepared at pH 5 had a liquid limit of 69%.

It is worth noting that during the determination of the liquid limit for the alkaline sample, it was not possible to have a level surface, as the samples tended to form a convex surface (Figure 8). Figure 8a, shows the alkaline sample, where a clear bulge is visible, whereas in Figure 8b, the top surface of the acidic sample is almost perfectly flat (Figure 8b). This phenomenon was associated with a tendency to swell in the alkaline sample, caused by a higher level of particle alignment when compared with the acidic sample.

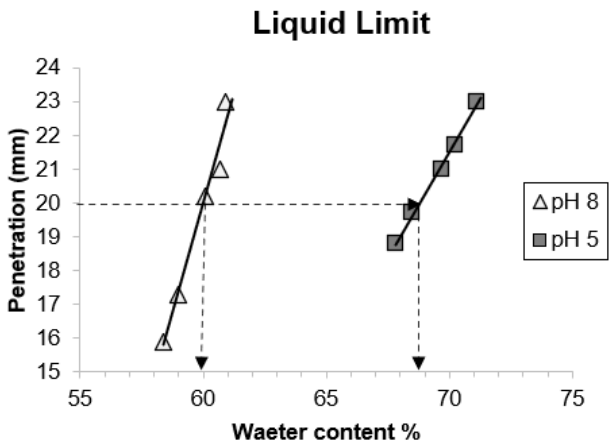

Figure 7: Liquid *Limit of fine muscovite at a) pH 8 and b) pH 5*

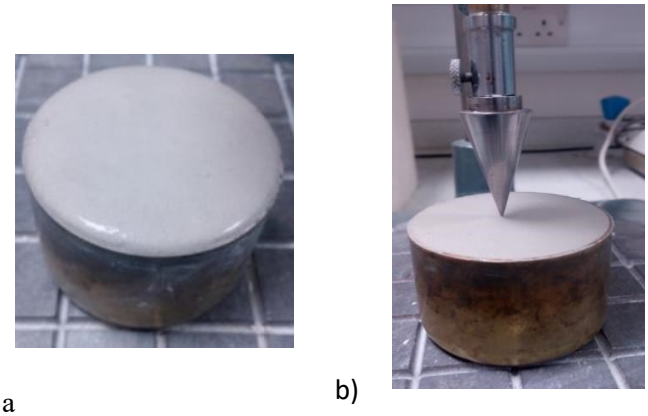

a b)

Figure 8: a) Convex muscovite silt surface (pH 8) in a penetrometer cup b) mica silt mixed with acidified water (pH 5) with flat surface in a penetrometer cup.

3.3 Jet erosion test

Two different sets of compacted mica samples prepared at differing pH (either pH 5 or 8) were tested for erosion susceptibility by means of the jet erosion test. Each set of samples was compacted at a different moisture content (e.g., 0.2, 0.3, and 0.4), and each sample was reproduced in triplicate, resulting in a total of 9 tests at pH 5 and 9 tests at pH 8.

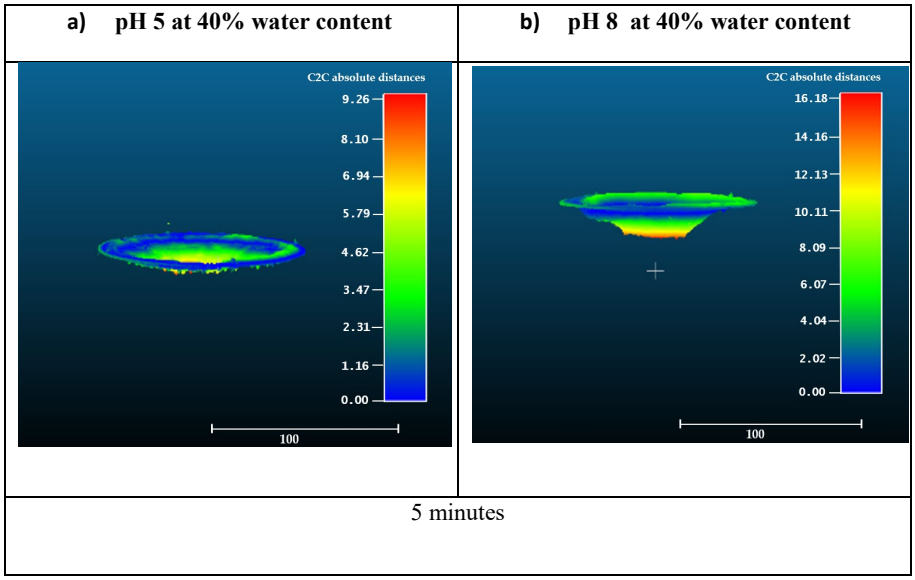

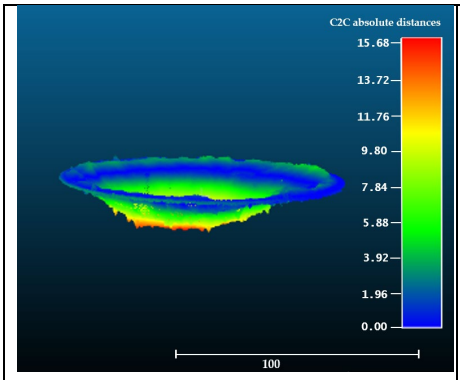

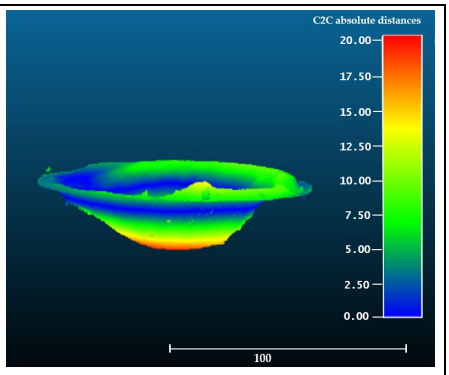

10 minutes

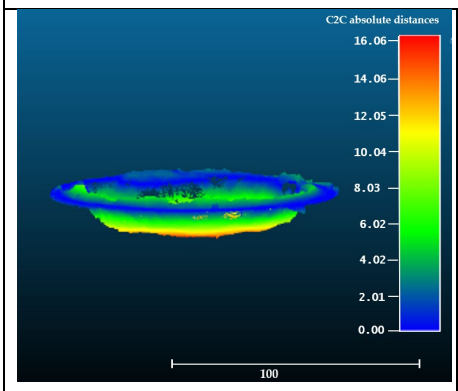

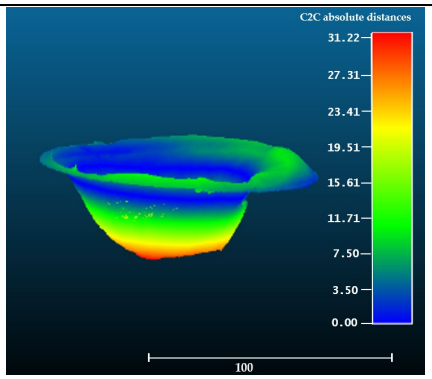

15 minutes

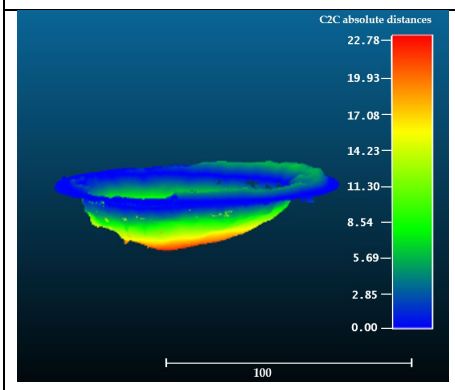

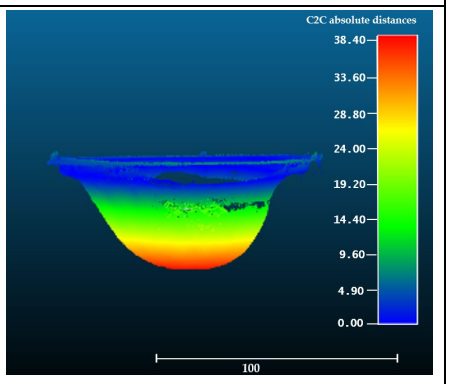

20- minutes

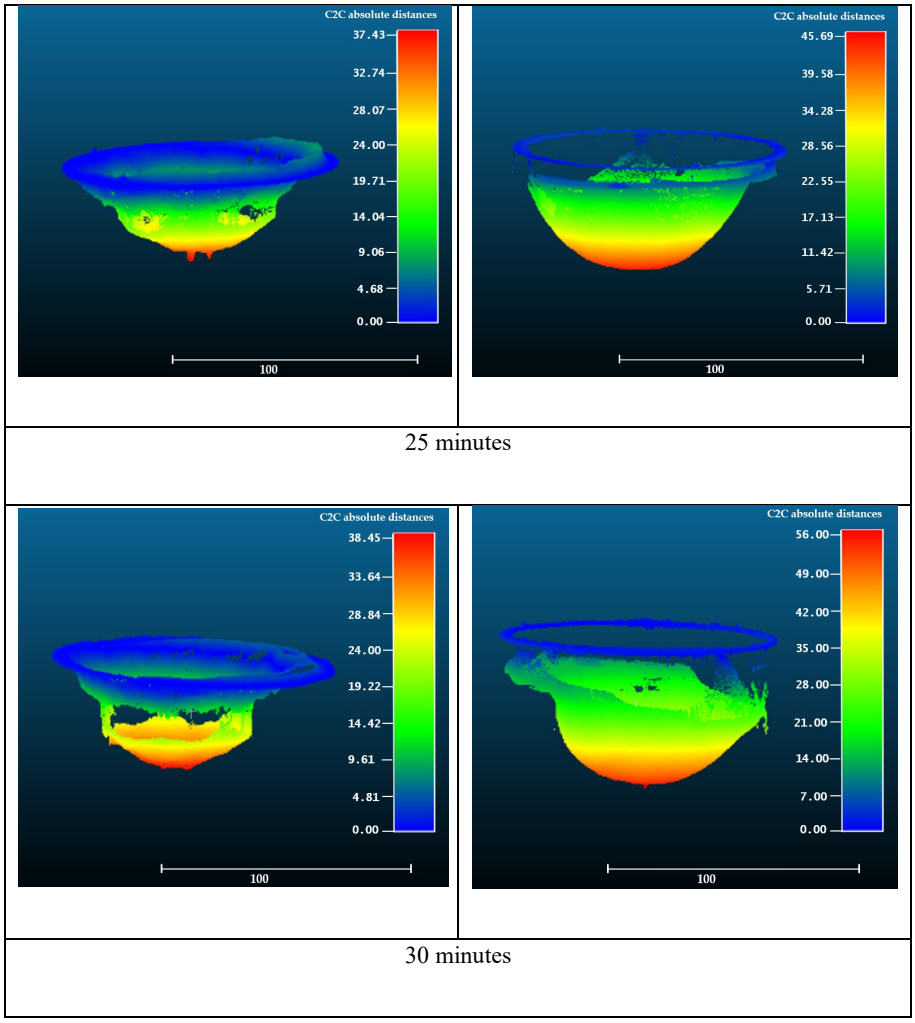

Figure 9: Jet erosion test eroded surfaces. a) pH 5 at 40% water content, b) pH 8 at 40% water content

In Figure 9 the scans of the eroded surface at the end of each jet time interval (5 minutes) are shown for two samples compacted at a moisture content of 0.40. Figure 9a shows results for the sample prepared at pH 5 and Figure 9b at pH 8. Each row in Figure 9 contains the scans of the eroded surfaces, for jet erosion times of 5, 10, 15, 20, 25 and 30 minutes. The colour bars are blue for the shallowest scour depths, with a progressive increase through green – yellow and then red as the depth of scour increase (reported in millimetres).

For all the scans, the scour surface has a bell shape, that was centred under the nozzle of the jet. For both tests, as expected, the volume of scoured material increases, and the scour surface depth increases, with increasing time. For the same jet erosion time, the pH 5 sample (Figure 9a) has a consistently smaller scour depth than the pH 8 sample (Figure 9b). For example, after

5 minutes, the pH 5 sample has a maximum scour depth of 9 mm, whereas the pH 8 sample has a maximum scour depth of 16 mm.

In Figure 10a, 10b and 10 c, the evolution of the maximum scour depth over time is reported for moisture contents of 0.2, 0.3 and 0.4, respectively. Each point corresponds to the median value of the triplicates and the error bars represent the range.

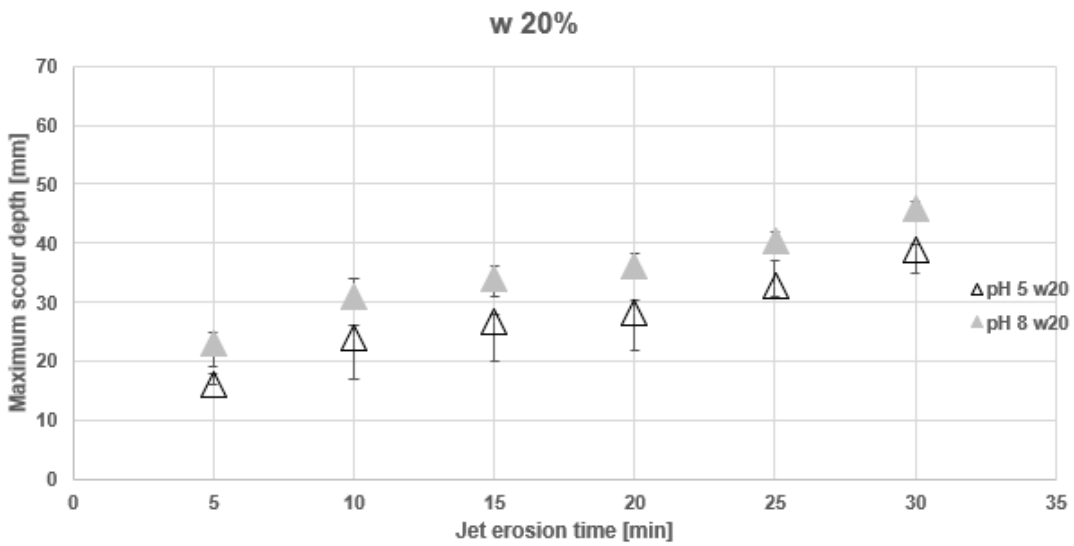

a)

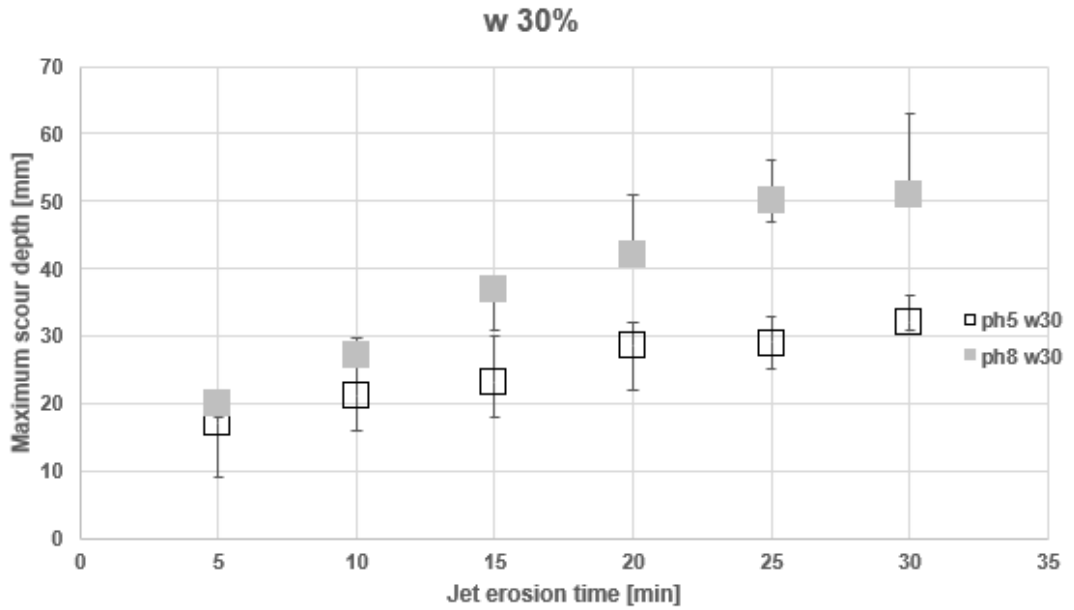

b)

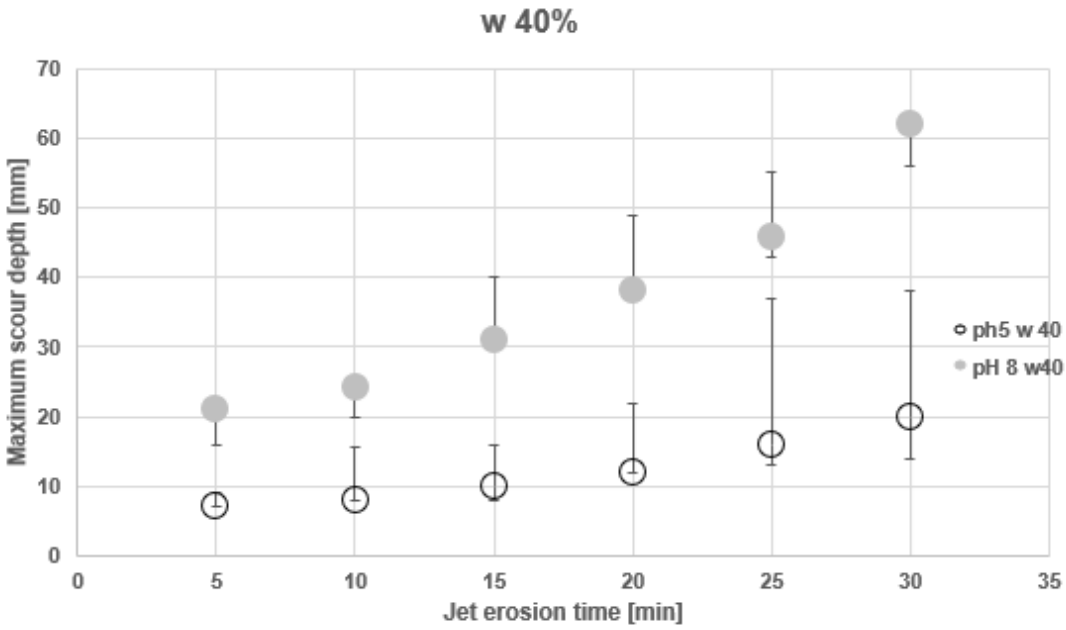

c)

Figure 10: Maximum scour depth. a) samples compacted at 20% moisture content, b) samples compacted at 30% moisture content and c) samples compacted at 40% moisture content

Samples compacted with alkaline water content are persistently more erodible (higher maximum scour depth) than samples compacted with acidic water content (Figure 10). Further, the higher the compaction moisture content the greater the difference in median scour depth between the acidic and the alkaline samples. For example, after 30 minutes of jet erosion, the difference in maximum median depth for the samples compacted at 0.20 was 7 mm, for the samples compacted at 0.30 was 19 mm and for the samples compacted at 0.40 was 42 mm.

The erosion data were elaborated by considering the model presented by **Hanson & Cook, (2004)**, where the erosion rate ε [m/s] (equation 1) is assumed to be proportional to both the soil's erodibility coefficient k_D [m/s/Pa] and the excess of the applied shear stress τ at the surface at critical shear stress, τ_c [Pa] (Karamigolbaghi et al., 2017).

$$\varepsilon = k_D(\tau - \tau_C) \quad (1)$$

For each test, the critical shear stress, τ_C (equation 2), was calculated according to the theory exposed by Blaisdell in 1981, originally proposed for the scour depth of the bridge piers

(Karamigolbaghi et al., 2017). In equation 2, τ_0 is the maximum shear stress of the jet, J_E is the nozzle height from the scour surface and J_P is the potential core length where the mean centerline velocity of the jet remains the same as that exiting from the nozzle (calculated considering a friction coefficient of 6.3 and an iterative process). According to the presented theory, the critical shear stress, τ_C, is meant as the threshold shear stress at which the "*first detachment*" occurs, hence when erosion starts. In other words, below that threshold value, no erosion is occurring.

$$\tau_c = \tau_0 (\frac{J_P}{J_E})^2 \quad (2)$$

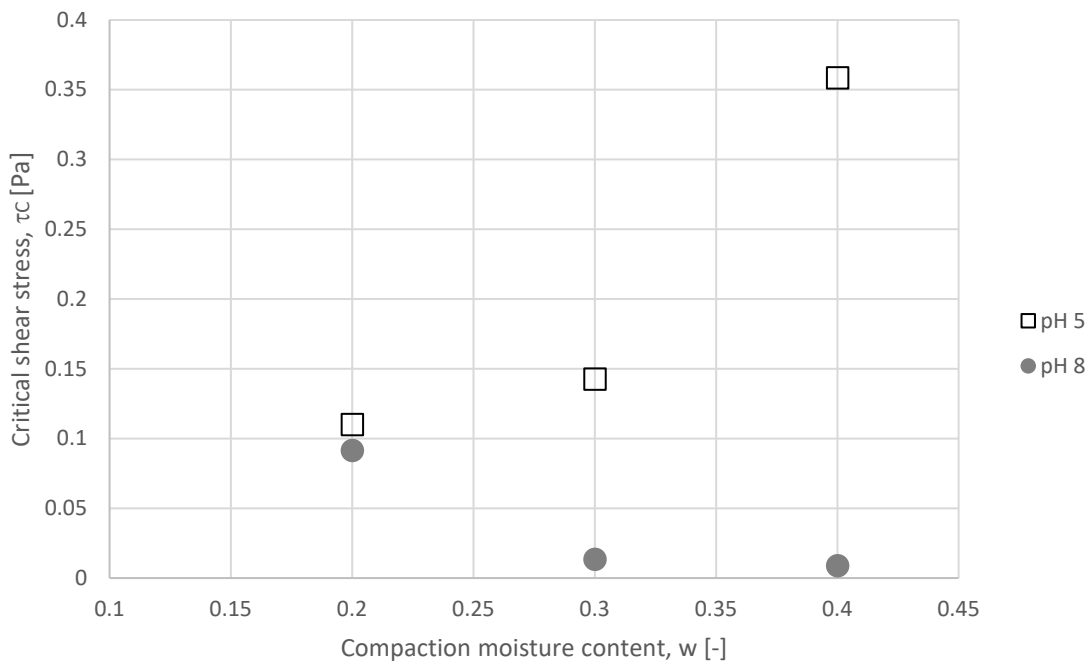

Figure 11. Critical shear stress

In Figure 11 the average value of the critical shear stress, τ_C, is plotted, as derived from the triplicate test, for each combination of pH and compaction moisture content. The critical shear stress of the alkaline samples decreases as the compaction moisture content increases. By contrast, the critical shear stress of the acidic samples increases as the compaction water content increases. At low values of the compaction moisture content, both the alkaline and the acidic

samples have a similar critical shear stress, of about 0.1 Pa. For the alkaline samples, this rapidly decreases to zero as the compaction moisture content increase. For the acidic samples, doubling the initial moisture content results in an increase in the critical shear stress of more than three times (from 0.11 Pa for a moisture content of 0.20 to 0.36 Pa for a moisture content of 0.40)

3.4 An electrochemical conceptual model for mica

Sedimentation tests show that particle configuration and interaction can be modified by changing the pore water chemistry. When mixed with distilled water, muscovite has an alkaline pH with relatively low sedimentation height and no clear water- suspension interface. This is indicative of a dispersive particle arrangement. On adjusting the pore fluid to acidic conditions (at low ionic concentrations – less than 0.1mol/l) the particles show a clear water- suspension interface and the settling time reduces. This is indicative of a non-dispersive fabric (flocculated or aggregated). In addition, at a high ionic concentration, for all pHs considered non-dispersive behaviour was the dominant fabric mode.

The dispersive nature of fine muscovite at alkaline pH and low ionic concentration was further confirmed by the difficulty observed (the convex bulging surface of muscovite slurry in a penetrometer cup) in the determination of the muscovite liquid limit at low ionic concentration and high pH. A flat surface of muscovite slurry was only obtained for a moisture content that was close to the liquid limit when acidic pore fluid was used to prepare the slurry (non-dispersed, aggregated/flocculated fabric).

The aggregation of clay particles in colloidal suspension is generally controlled by the net balance between the mutual repulsion, due to the negative electrical charge of the surface, and the surface attraction due to the presence of surface forces such as Van der Waals forces. The repulsion between two charged surfaces is proportional to the electrical charge (or electric

potential) at the surface and inversely proportional to the dielectric constant of the medium between the surfaces.

Mica particles, when in suspension in water, are generally considered to have a negative charge distributed on their surface. This negative charge generates an electrical repulsion which depends on the physical properties of the dispersing media. Simultaneously, when a small distance exists between two facing surfaces, a Van der Waals attraction is instead generated, by the electron interaction of the two surfaces (Hamaker, 1937; Casimir and Polder, 1948) In a clay suspension, the interaction force existing between two particles at a given distance is given by the net energy resulting from the balance between the electrical repulsion and the Van der Waals attraction. For clays in suspension in water, this is generally assumed to be negative (repulsive) unless the chemistry of the suspension is altered. The aggregation rate between negatively charged particles is controlled by the repulsive interaction force and the kinetic energy resulting from their Brownian motion. If the repulsive barrier existing between two particles is high enough not to be overcome by the Brownian motion, the two particles will remain in a dispersed state, and settle individually. On the other hand, if by altering the chemistry of the suspension, and hence the charge of the particle surface, the negative repulsive barrier is depleted, the particles in suspension will have enough kinetic energy to overcome such a barrier, and aggregate/flocculate. These particles will therefore tend to settle as a cluster of one or more particles.

When dispersed in neutral water, mica tends to increase the pH of the solution toward a pH of around 8 or 9. It is reasonable to assume that this is the pH of pore water when in equilibrium with the mica, unless altered. In this condition, the surface of mica particles are highly negative: z potential about -140 mV (Nishimura et al., 1992). When the pore water of mica is altered in order to decrease the pH below 5, the zeta potential decreases sharply. At pH 4 the z potential is about -70 mV (Nishimura et al., 1992). The change in the negative potential at the particle

surface **and edge** is directly proportional to the change in repulsion between two facing particles of mica. This change in the mica particle repulsion results in the observed change to the mica settling pattern when the pH drops from 9 to 5 (Figure 6a). It seems reasonable and consistent to assume that mica particles at pH 5 are settling in an aggregate/flocculated mode (non-dispersed). This hypothesis is strongly corroborated by the observations that: i) at pH 9 the water suspension never becomes clear, implying that smaller particles do not settle, and ii) the final volume of the sediment for the sample at pH 5 is higher than that at pH 9.

In addition, research by Zhao et al., (2008) and Yan et al., (2011) using direct colloid probe force measurement and atomic force microscope measurement respectively suggest that the basal plane of muscovite mica carry a permanent negative charge while the edge charge is pH dependent (with positive edge charge at lower pH and negative edge charge at higher pH range). This further supports additional interaction and flocculation between particles in the acidic pH range and dispersion in the alkaline pH range.

The energy barrier between particles can be also depleted by increasing the electrolyte concentration of the suspension. As explained by the well-known the DLVO theory (Guoy 1910, Deraguin and Landau 1941, Verwey and Overbeek 1948), the cations dissolved in water are shielding the electrical charge of the particle surface and therefore reducing its negative repulsion. Consequently, when the electrolyte concentration is increased, the particle repulsion becomes smaller and therefore the probability that two particles will aggregate/flocculate increases. Figure 6c and d, showed that, at 0.1M and 1.8 M concentration of KCl, the sedimentation times are all very similar, regardless of the pH and the KCl concentration. It seems reasonable to assume that at this electrolyte concentration, the shielding effect of the cations present in the double layer is so high that the charge (or potential) at the surface no longer matters and the negative repulsion is entirely depleted. Hence, the Van der Waals attraction dominates.

Although distinguishing whether mica associates in flocs, or in aggregates made of parallel particles, is out of the scope of this research work it is worth noting that the sedimentation curves reported in figure 6 for the non-dispersed samples are the same regardless of the way the suspension was destabilized (pH or ionic strength). This implies that the association mode is the same (i.e., either one or the other). Indeed, one might expect that aggregates and flocs with different sizes and densities would return a different final void ratio for the sediment and a different settlement velocity. The experimental evidence presented here is somehow in contrast with the common understanding that, for clay suspension, flocculation is generally attributed to acidic destabilization at low ionic strength, and aggregation to destabilization caused by high ionic strength. However, whatever the association process, the experimental evidence suggests that for the case of non-dispersed sedimentation, particles interaction is attractive.

The strength of mica samples in a dispersed configuration (pH 9 and low ionic strength) and a non-dispersed configuration (either pH 5 or high ionic strength) was compared using the liquid limit test. The non-dispersed samples were stronger, with a higher liquid limit, than the dispersed ones. These findings are consistent with the experimental results reported by **Pedrotti, (2016)** for kaolin clay at different particle configurations, where the liquid limit was found to increase with the average floc size within the sample. Again, these results suggest that the unit elements within the acidic mica samples are not single particles, but groups of particles clustered together.

In the 70s, Moore and Mitchell, (1974) first, and van Olphen (1977) after, showed that the shear strength of a clay sample is proportional to the net attraction existing between particles. Moore and Mitchell, (1974) proved it by measuring the undrained shear stress of clay samples with differing van der Waals interaction, whereas van Olphen (1977) demonstrated it by measuring the Bingham stress of a suspension with different aggregate patterns. Accordingly,

the results obtained here for the liquid limit (Figure 7), show that acidic samples, where particle interaction is attractive in nature, have a higher liquid limit than alkaline ones.

3.5. An electrochemical conceptual model for the erosion of mica

The increase in shear strength for the non-dispersed mica samples is also reflected in the erosion susceptibility tests.

Shields in 1936 performed a set of experimental tests on coarse soil, which for the following century has been considered as the benchmark dataset to develop theories and to characterize soil erosion susceptibility. As the soil tested by Shield was coarse and non-cohesive, the main assumption adopted in the many theories developed to interpolate his data, is that there is no electrochemical interaction forces between particles. When soil is eroded, single particles are detached from the soil mass by drag and lift forces, without creating any shear stress on the bed (Miedema, 2013). By contrast, a cohesive sediment, is subject to the phenomena where particles interact with each other. In Figure 12, the function developed by Soulsby and Whitehouse (1997), to interpolate Shields dataset for coarse material is shown (black solid line). The same curve has been extrapolated (black dashed line), using his equation in the range for smaller particle diameters (silt-size), in order to compare it with the experimental dataset presented in this research. In the same figure, the function derived by **Lick et al. (2004)** is also reported for a reference compaction density of ~ 1.5 [g/cm3]. **Licket al. (2004)** developed this function (grey solid line in Figure 12) to account for the particle interaction that develops in finer materials. To allow a fit to the Shields dataset in the range of coarse material, a cohesive factor, inversely proportional with the particle size is introduced by **Lick et al. (2004)**. Soulsby and Whitehouse (1997) curves provide a reference behaviour for the erosion mechanisms of interacting and non-interacting particles i.e., for soils with cohesion and for cohesionless behavior, respectively.

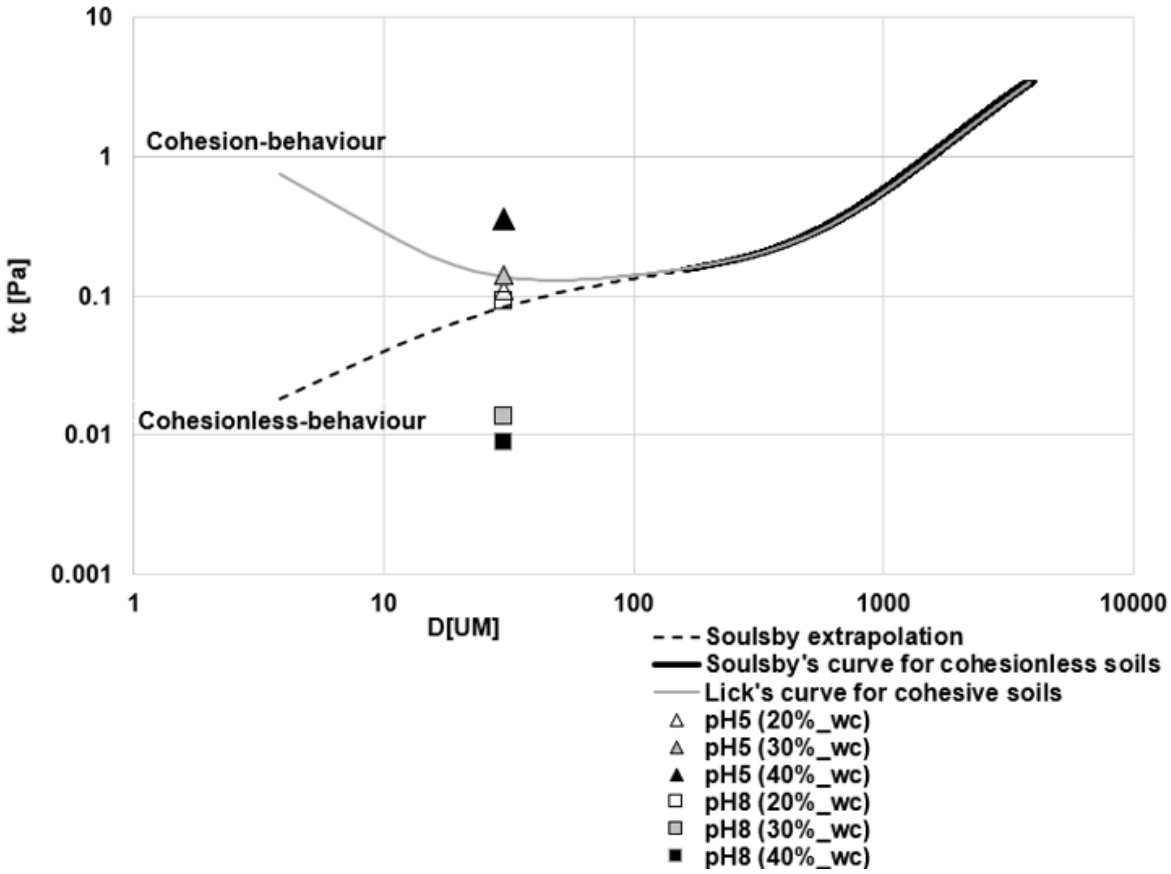

Figure 12: Shields curve

In Figure 12, the two curves are plotted along with the six sets of erosion experimental data presented in Figure 10. It is interesting to note that at low compaction moisture contents, both the acidic and alkaline samples have a τc of about 0.1 Pa, and the two points lie quite close to Soulsby's curve for cohesionless soils. As the compaction moisture content is increased both datasets (e.g. acidic and alkaline sample) move away from Soulsby's curve. As the alkaline water content at compaction is increased, the critical shear stress reduces, and the data points end up well below Soulsby's curve for cohesionless soils. As the number of particles in contact with alkaline water increases, the more particles are interacting in a dispersive fashion, the particles are therefore becoming more prone to erosion, hence less force is required to lift them. As shown in Figure 13a, it is suggested that for dispersed samples, erosion occurs in a particle-by-particle fashion, as generally assumed for a cohesionless coarse material. By contrast, for the acidic samples, as the number of particles in contact with acidic water increases, the more

particles are interacting in an attractive fashion, and the associated erosion critical shear stress moves towards and above Lick's curve for cohesive soils. Once the particle attraction is activated, the elementary unit within the soil is no longer a single particle, but a cluster of them (erosion of non-dispersed particle configuration in Figure 13b). This results in a higher shear stress at the surface. It is interesting to note that the critical shear stress of a sample of mica particle, with an average diameter of 30 mm when compacted with acidic water to a moisture content of 0.40, corresponds to a critical shear stress of a coarse material having a grain size of about 0.7 mm.

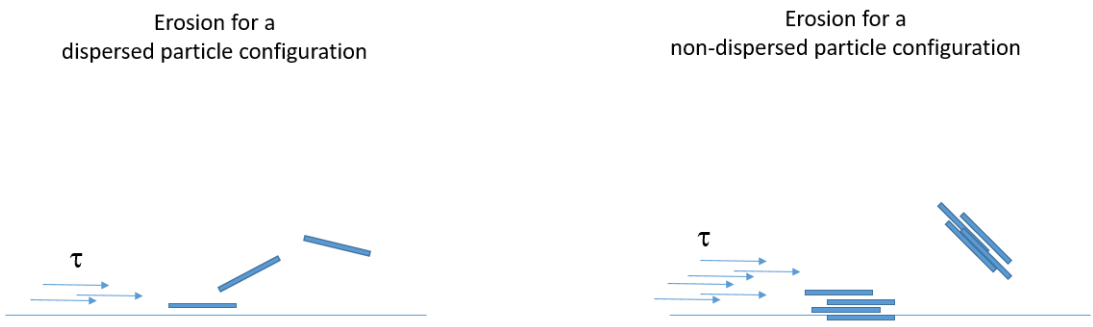

Figure 13: Conceptual model of mica particle erosion at a) dispersed particle configuration and b) non-dispersed particle configuration

Although, the test conducted here is a small-scale laboratory test which will require further refinement, the result suggest that it may be possible to enhance muscovite silt stability through adequate pore-water acidification. This may be particularly useful in relatively low stress applications such as the use of mica as an alternative source of potassium (which plays an important role in several physiological processes in plant nutrition) or as a fill material for embankment.

3.6. Environmental considerations about the use of mica for agricultural applications

This work suggests that acidification of pore-water contributes to stabilising the mica-based material against water-induced erosion. It is worth highlighting that the values of pH required to achieve stability falls within the range of pH values encountered in agricultural applications. Crop plants vary in their tolerance to acidity and plant nutrients have different optimal pH ranges (Goulding, 2016). For example, ericaceous (lime-hating) plants such as rhododendrons, camellias, heathers, azaleas, blueberries, white potatoes and conifer trees do well in acidic soil in the range of pH 5 to pH 6. Similarly, normal rain is usually slightly acidic, with a pH of between 5 and 5.6 (Goulding, 2016) due to the dissolution of carbon dioxide (CO_2) and the dissociation of the resulting carbonic acid (H_2CO_3). Soil usually attains the same equilibrium pH as that of the rain to which it is exposed. Hence, natural soil conditions will generally provide a good environment for mica-enhanced erosion resistance as well as providing a source of potassium for ericaceous plants.

Considering mica as a source of potassium, there is a need to further evaluate the best possible environmental conditions for the release of potassium by mica. However, studies by **Biswas & Basak, (2014); Meena et al. (2015); Singh et al. (2010)** showed that potassium can be released favourably under a wide range of non-stringent environmental conditions, for example variation in temperature and moisture content did not affect the rate of mobilisation of K. They demonstrated that the addition of potassium solubilising rhizobacteria to waste mica for k mobilisation significantly enhanced the release of K ions and resulted in the release of organic acid, stabilising the pH of the system to a pH of between about 5 and 7. This is consistent with the desired pH range for enhanced erosion resistance.

4. Conclusion

This paper presents an experimental campaign to characterize mica erosion susceptibility. Mica particle-to-particle interaction forces and their effect on the macroscopic behaviour were

systematically investigated by changing the pore fluid pH and ionic concentration. Results from sedimentation tests and liquid limit tests have informed a conceptual model of the mica fabric that is able to explain the enhanced erosion resistance under acidic and/or high ionic concentration pore-water conditions.

It is shown that the particle configuration of mica samples consistently varies with the pore water chemistry, regardless of whether the samples being tested were suspension sediments or compacted samples. For mica samples formed with neutral water at low ionic concentration, the particles are in a dispersed configuration. This implies a poor mechanical behaviour and high erosion susceptibility, as particles are eroded one by one. When the mica pore chemistry is altered, however, either by acidification or by an increase in the ionic strength, particles tend to cluster together and organize in a non-dispersed configuration. This results in an improved mechanical behaviour and less erosion susceptibility, as group of particles must be eroded as opposed to individual ones.

Although the water chemistry has been shown to change the particle configuration, the experimental findings suggest this may only occur when the water chemistry is altered at sample formation. The water used in the jet for all erosion tests was neutral water, but it did not result in a change to sample behaviour over time. To confirm the effect of infiltration water chemistry, further investigation is needed.

Considering that mica waste is derived from mining operations, which are often slightly acidic due to some metal content (e.g., iron sulphides which result in the leaching of sulphuric acid), the work presented in this paper paves the way for tailored assessments of individual mica waste materials to determine the appropriateness of their use.

5. Acknowledgement

The publication of this work was made possible through support from the University of Strathclyde Research Studentship.

6. Data Availability Statement

Some or all data, models, or code that support the findings of this study are available from the corresponding author upon reasonable request.

7. Reference

Bakken, A. K., Gautneb, H., & Myhr, K., 1997. The potential of crushed rocks and mine tailings as slow-releasing K fertilizers assessed by intensive cropping with Italian ryegrass in different soil types. *Nutrient Cycling in Agroecosystems*, *47*, 41–48.

Basak, B. B., 2019. Waste Mica as Alternative Source of Plant-Available Potassium: Evaluation of Agronomic Potential Through Chemical and Biological Methods. *Natural Resources Research*, *28*(3), 953–965. https://doi.org/10.1007/s11053-018-9430-3

Basak, B. B., Sarkar, B., Biswas, D. R., Sarkar, S., Sanderson, P., & Naidu, R., 2017. Bio-Intervention of Naturally Occurring Silicate Minerals for Alternative Source of Potassium: Challenges and Opportunities. *Advances in Agronomy*, *141*, 115–145. https://doi.org/10.1016/bs.agron.2016.10.016

Beber, R., Tarantino, A., Pedrotti, M., & Lunn, R. J., 2019. The effect of clay water content in the jet erosion test. *E3S Web of Conferences*, *92*. https://doi.org/10.1051/e3sconf/20199202016

Biswas, D. R., & Basak, B. B., 2014. Mobilization of potassium from waste mica by potassium-solubilizing bacteria (Bacillus mucilaginosus) as influenced by temperature and incubation period under in vitro laboratory conditions. *Agrochimica*, *58*(4), 309–320. https://doi.org/10.12871/0021857201442

BS, P., 1990. "7: 1990. British Standard Methods of Test for Soils for Civil Engineering Purposes, Part 7: Shear strength tests (total stress) tests." British Standards Institution, London.

Casimir, H.B. and Polder, D., 1948. The influence of retardation on the London-van der Waals forces. Physical Review, 73(4), 360. https://doi.org/10.1103/PhysRev.73.360

Cresswell, D. and Sims, V., 2007. "Characterisation of mineral wastes, resources and processing technologies—Integrated waste management for the production of construction material." Case Study: Green roof substrate using aerated concrete waste. Report WRT 177/WR0115 (October) issued by University of Leads, Akristos, and Mineral Industry Research Organisation. DEFRA (Department for Environment, Food, and Rural Affairs), UK.

Deraguin, B. and Landau L., 1941. "Theory of the stability of strongly charged lyophobic sols and of the adhesion of strongly charged particles in solution of electrolytes." Acta Physicochim: USSR 14: 633-662.

Dudeney, A. W. L., Chan, B. K. C., Bouzalakos, S., & Huisman, J. L., 2013. Management of waste and wastewater from mineral industry processes, especially leaching of sulphide resources: State of the art. *International Journal of Mining, Reclamation and Environment*, *27*(1), 2–37. https://doi.org/10.1080/17480930.2012.696790

Goulding, K. W. T., 2016. Soil acidification and the importance of liming agricultural soils with particular reference to the United Kingdom. *Soil Use and Management*, *32*(3), 390–399. https://doi.org/10.1111/sum.12270

Guoy, G., 1910. "Constitution of the electric charge at the surface of an electrolyte." J Physique 9: 457-467.

Gratchev, I., & Towhata, I., 2013. Stress-strain characteristics of two natural soils subjected to long-term acidic contamination. *Soils and Foundations*, *53*(3), 469–476.

https://doi.org/10.1016/j.sandf.2013.04.008
Hamaker, H. C., 1937. The London-van der Waals attraction between spherical particles. *Physica*, *4*(10), 1058–1072. https://doi.org/10.1016/S0031-8914(37)80203-7
Hanson, G. J., & Cook, K. R., 2004. Apparatus, test procedures, and analytical methods to measure soil erodibility in situ. *Applied Engineering in Agriculture*, *20*(4), 455–462.
Hanson, G. J., & Simon, A., 2001. Erodibility of cohesive streambeds in the loess area of the Midwestern USA. *Hydrological Processes*, *15*(1), 23–38. https://doi.org/10.1002/hyp.149
Hojamberdiev, M., Eminov, A., & Xu, Y., 2011. Utilization of muscovite granite waste in the manufacture of ceramic tiles. *Ceramics International*, *37*(3), 871–876. https://doi.org/10.1016/j.ceramint.2010.10.032
Hoseini, S. M. R., Bahrami, A., & Hosseinzadeh, M., 2016. The reclamation of mica flakes from tailing disposal using gravity separators and flotation. *International Journal of Mining and Geo-Engineering*, *50*(1), 61–76. https://doi.org/10.22059/IJMGE.2016.57309
Karamigolbaghi, M., Ghaneeizad, S. M., Atkinson, J. F., Bennett, S. J., & Wells, R. R., 2017. Critical assessment of jet erosion test methodologies for cohesive soil and sediment. *Geomorphology*, *295*(March), 529–536. https://doi.org/10.1016/j.geomorph.2017.08.005
Karlsson, T., Kauppila, P., & Lehtonen, M., 2017. *Assessment of the effects of mine closure activities to waste rock drainage quality at the Hitura Ni-Cu mine, Finland*. Proceedings of the 13th International Mine Water Association Congress–"Mine Water & Circular Economy–A Green Congress", 80–87.
Keesstra, S. D., Bouma, J., Wallinga, J., Tittonell, P., Smith, P., Cerdà, A., Montanarella, L., Quinton, J. N., Pachepsky, Y., Van Der Putten, W. H., Bardgett, R. D., Moolenaar, S., Mol, G., Jansen, B., & Fresco, L. O., 2016. The significance of soils and soil science towards realization of the United Nations sustainable development goals. *Soil*, *2*(2), 111–128. https://doi.org/10.5194/soil-2-111-2016
Lick, W., Jin, L., & Gailani, J., 2004. Initiation of Movement of Quartz Particles. *Journal of Hydraulic Engineering*, *130*(8), 755–761. https://doi.org/10.1061/(asce)0733-9429(2004)130:8(755)
Liu, J., Gao, G., Wang, S., Jiao, L., Wu, X., & Fu, B., 2018. The effects of vegetation on runoff and soil loss: Multidimensional structure analysis and scale characteristics. *Journal of Geographical Sciences*, *28*(1), 59–78. https://doi.org/10.1007/s11442-018-1459-z
Lottermoser, B., 2010. Mine Wastes: Characterization, treatment and environmental impacts. Mine Wastes: Characterization, Treatment and Environmental Impacts.
Man, A., & Graham, J., 2010. Pore fluid chemistry, stress-strain behaviour, and yielding in reconstituted highly plastic clay. *Engineering Geology*, *116*(3–4), 296–310. https://doi.org/10.1016/j.enggeo.2010.09.011
Meena, V. S., Maurya, B. R., Verma, J. P., Aeron, A., Kumar, A., Kim, K., & Bajpai, V. K., 2015. Potassium solubilizing rhizobacteria (KSR): Isolation, identification, and K-release dynamics from waste mica. *Ecological Engineering*, *81*(August), 340–347. https://doi.org/10.1016/j.ecoleng.2015.04.065
Miedema, S.A., 2011. Constructing the shields curve. International Conference on Offshore Mechanics and Arctic Engineering, 44397, 825-840. https://doi.org/10.1115/OMAE2011-49232
Mitchell, J. K., & Soga, K., 2005. Fundamentals of Soil Behavior. In *Soil Science*, 158(1). https://doi.org/10.1097/00010694-199407000-00009
Momeni, M., Bayat, M., & Ajalloeian, R., 2020. Laboratory investigation on the effects of pH-induced changes on geotechnical characteristics of clay soil. *Geomechanics and Geoengineering*, 1–9. https://doi.org/10.1080/17486025.2020.1716084
Moore, C. A., & Mitchell, J. K., 1974. Electromagnetic Forces and Soil Strength. *Geotechnique*, *24*(4), 627–640. https://doi.org/10.1680/geot.1974.24.4.627
Nishimura, S., Tateyama, H., Tsunematsu, K., & Jinnai, K., 1992. Zeta potential measurement of muscovite mica basal plane-aqueous solution interface by means of plane interface technique. *Journal of Colloid And Interface Science*, *152*(2), 359–367. https://doi.org/10.1016/0021-9797(92)90038-N
Nosrati, A., Addai-Mensah, J., & Skinner, W., 2009. pH-mediated interfacial chemistry and particle interactions in aqueous muscovite dispersions. *Chemical Engineering Journal*, *152*(2–3), 406–

414. https://doi.org/10.1016/j.cej.2009.05.001

Palomino, A. M., & Santamarina, J. C., 2005. Fabric map for kaolinite: Effects of pH and ionic concentration on behavior. *Clays and Clay Minerals*, *53*(3), 211–223. https://doi.org/10.1346/CCMN.2005.0530302

Palumbo-Roe, B., Colman, T., Cameron, D. G., Linley, K., & Gunn, A. G., 2014. *The nature of waste associated with closed mines in England and Wales*. 82. http://nora.nerc.ac.uk/id/eprint/10083/ (accessed 15 September 2020).

Pedrotti, M., 2016. *An experimental investigation on the micromechanisms of non-active clays in saturated and partially saturated states*. PhD Thesis submited to the Department of Civil and Environmental Engineering, University of Strathclyde.

Singh, G., Biswas, D. R., & Marwaha, T. S., 2010. Mobilization of potassium from waste mica by plant growth promoting rhizobacteria and its assimilation by maize (Zea mays) and wheat (Triticum aestivum L.): A hydroponics study under phytotron growth chamber. *Journal of Plant Nutrition*, *33*(8), 1236–1251. https://doi.org/10.1080/01904161003765760

Sinha, N., Deb, D., & Pathak, K., 2017. Development of a mining landscape and assessment of its soil erosion potential using GIS. *Engineering Geology*, *216*, 1–12. https://doi.org/10.1016/j.enggeo.2016.10.012

Soulsby, R. and Whitehouse R., 1997. Threshold of sediment motion in coastal environments. Pacific Coasts and Ports' 97: Proceedings of the 13th Australasian Coastal and Ocean Engineering Conference and the 6th Australasian Port and Harbour Conference;Centre for Advanced Engineering, University of Canterbury. 1, 145-150.

van Olphen, H., 1977. An introduction to clay colloid chemistry, for clay technologists, geologists, and soil scientists. 2nd Edition, Wilwy, New York.

Verwey, E. J. W., & Overbeek, J. T. G., 1948. Theory of the stability of lyophobic colloids. In Journal of Colloid Science (Vol. 10, Issue 2, pp. 224–225). https://doi.org/10.1016/0095-8522(55)90030-1

Wang, A., Li, X., Huang, Z., Huang, X., Wang, Z., & Wu, Q., 2015. Laboratory study on engineering geological characteristics and formation mechanism of altered rocks of Henan Tianchi pumped storage power station, China. *Environmental Earth*, 5063–5075. https://doi.org/10.1007/s12665-015-4520-6

Wang, H., & Zhang, G. H., 2021. Temporal variation in soil erodibility indices for five typical land use types on the Loess Plateau of China. *Geoderma*, *381*, 114695. https://doi.org/10.1016/j.geoderma.2020.114695

Zografou, A., Heath, A., & Walker, P., 2014. China clay waste as aggregate in alkali-activated cement mortars. *Proceedings of the Institution of Civil Engineers - Construction Materials*, *167*(6), 312–322. https://doi.org/10.1680/coma.13.00037